Determination of polarizabilities and lifetimes for the Mg, Zn, Cd and Hg isoelectronic sequences

Nicholas Reshetnikov[1], Lorenzo J Curtis, Michael S Brown and Richard E Irving

Department of Physics and Astronomy, University of Toledo, Toledo, OH 43606, USA

E-mail: ljc@physics.utoledo.edu

Abstract

The dipole polarizability and adiabatic correlations of atomic ions are related to the energy levels and oscillator strengths of the levels through bracketing inequalities. For systems with a ground state $ns^2\ {}^1S_0$, the total oscillator strength is dominated by the unbranched intrashell $ns^2\ {}^1S_0$–$nsn p\ {}^1P^o_1$ transition, and the remaining oscillator strength can be narrowly bracketed using the f-sum rule. Thus measurements of the lifetime of the lowest resonance transition can be used to specify the polarizabilities and, alternatively, measurements of the polarizabilities can be used to deduce lifetimes. Moreover, isoelectronic regularities in line strengths can be used to obtain a comprehensive database from a small number of precision lifetime determinations. These methods are applied homologously to produce values for polarizabilities and lifetimes for the Mg, Zn, Cd and Hg isoelectronic sequences. To confirm the reliability of these methods, fast ion beam lifetime measurements in P IV were performed using the arbitrarily normalized decay curve (ANDC) method, and a test of the f-sum was made for Ba II, for which precision measurements of both the polarizability and lifetimes exist.

PACS numbers: 32.70.Cs, 32.10.Dk, 32.30.Bv

1. Introduction

Electric dipole polarizabilities α_d can be determined from spectroscopic studies of high Rydberg states, interpreted using the core polarization model [1]. Measurements of the energy levels of high n and ℓ states are modeled as a hydrogenlike-system with a deformable central core of charge. Effective polarizabilities of the core (one stage of ionization higher than the Rydberg ion) are then extracted as fitting parameters.

The quantity α_d can be theoretically formulated in terms of a sum and integral over factors involving the oscillator strengths f and energies E of excitations from the ground state to accessible bound and continuum excited states. In cases where these excitations are dominated by the lowest-lying (intrashell) resonance transition, this relationship can establish a lower bound for α_d. By invoking the f-sum rule, an upper bound can also be established, providing

a bracketing inequality [2] connecting α_d and f. The bracketing can be very tight if the intrashell excitation energy is significantly smaller than that of subsequent intershell resonance transitions.

This inequality provides an alternative method to determine α_d. If the dominant resonance transition is unbranched, the value of α_d can be accurately specified using a precision measurement of the lifetime τ of that transition. Similar relationships connect τ to the non-adiabatic correlation factor β (a measure of the inability of the core to follow the motion of the outer electron), which allow this quantity to be evaluated in the same manner.

In an application to Kr VII, it has recently been demonstrated [3] that significant improvements in the attainable accuracy of spectroscopic measurements now permit this procedure to be inverted, with experimental results for α_d used to specify values and uncertainty limits for f and τ. This can provide needed data in cases where direct decay curve measurements are hindered by, e.g. severe blending and cascading problems. We have extended this

---

[1] Present address: Department of Physics, Harvard University, Cambridge, MA 02138, USA.

inverse method utilizing existing precision polarizability data to obtain accurate values for lifetimes in Si III and P IV. Use of this approach also raises concerns about the reliability of earlier polarizability measurements in Pb III.

In order to verify the reliability of the prediction of lifetimes from polarizability measurements, a comprehensive set of fast ion beam decay curve measurements were made in P IV. These were subjected to analysis using the arbitrarily normalized decay curve (ANDC) method [4] to account for cascade repopulation. Also, to test the validity of the f-sum rule, a determination was made of the effective number of active electrons in Ba II, a system for which high precision measurements exist for both the polarizability and the lifetimes of the lowest resonance transitions.

Existing bases of semiempirically systematized lifetime data can be both utilized and enhanced by the use of these relationships between polarizabilities and lifetimes. Isoelectronic sets of lifetimes for unbranched transitions can be cleared of wavelength and intermediate coupling factors to yield a set of effective line strength factors. These factors have been found to produce a nearly linear isoelectronic plot when appropriately charge-scaled and plotted against a suitably-chosen reciprocal screened central charge. Thus a relatively small number of precision lifetime determinations can produce a reliable data set for the entire sequence by interpolation and extrapolation.

Through a systematic combination of the use of lifetimes determined from polarizabilities, polarizabilities determined from lifetimes, and isoelectronic expositions, a database for α_d, τ_{np}, and β is reported here for the Mg, Zn, Cd and Hg isoelectronic sequences. In addition, the isoelectronic database for α_d is used to investigate the charge scaling behavior, both to permit isoelectronic extrapolation and to study homologous trends.

2. Calculational formulation

We consider here ions with an ns^2 $^1S_0$ ground state outside a filled shell or filled subshell core. The oscillator strength $f_{ns,n'p}$ for the ground state excitation series ns^2 $^1S_0$–$nsn'p$ $^1P_1^o$ is dominated by the strong intrashell $n'=n$ transition. (For economy of notation, the explicit designation of the spectator ns electron will be suppressed.) The excitation energies $E_{ns,n'p}$ of these resonance levels are much higher for the intershell $\Delta n \neq 0$ cases than for the intrashell $\Delta n = 0$ case. The dipole polarizability of these ions will influence the energy levels of high Rydberg states in atoms and ions of the adjacent (one stage of ionization lower) isoelectronic sequence, from which α_d can be deduced using the long-range core polarization model [1].

Here equations will be expressed in atomic units, with energies in hartrees ($2 \times 109737.31568549 \ cm^{-1}$) and lengths in Bohr radii a_0 ($5.291772083 \ nm$). In standard notation, α denotes the fine structure constant ($1/137.03599976$) and c is the speed of light ($2.99792458 \times 10^8 \ nm \ ns^{-1}$).

2.1. Relationships among quantities

The quantum mechanical character of both the emission lifetime τ_{np} and the absorption oscillator strength $f_{ns,np}$ is

contained in the line strength factor $S_{ns,np}$ [5]

$$S_{ns,np} = S_{np,ns} = |\langle \Psi_{ns}|\mathbf{r}|\Psi_{np}\rangle|^2. \tag{1}$$

In the non-relativistic Schrödinger approximation, this quantity is the same for all members of the transition array between the two configurations, and differences among oscillator strengths and transition probabilities are a result of perturbations in level energies and intermediate coupling effects. The quantity $S_{ns,np}$ can either be computed theoretically or treated as an experimentally measured empirical parameter. For absorption from a $J = 0$ lower level, the oscillator strength is related to the line strength by [5]

$$f_{ns,np} = \tfrac{2}{3} E_{ns,np} \ S_{ns,np} \tag{2}$$

(quantities in au). For an unbranched $J = 1 \rightarrow 0$ transition, the lifetime τ_{np} is related to the oscillator strength by [5]

$$\frac{1}{\tau_{np}} = \frac{2c\alpha^4}{3a_0} E_{ns,np}^2 \ f_{ns,np}. \tag{3}$$

(Here $E_{ns,np}$ is in au, but c, a_0 and τ_{np} are in SI units to compare with experiment.)

The value of α_d for the ground state can be expressed in terms of $f_{ns,n'p}$ and $E_{ns,n'p}$ for the ns^2 $^1S_0$–$nsn'p$ $^1P_1^o$ Rydberg series through the relationship [2]

$$\alpha_d = \sum_{n'}^{\dagger} \frac{f_{ns,n'p}}{E_{ns,n'p}^2}. \tag{4}$$

The dagger on the summation indicates that this also includes an integral over continuum states. The f-sum rule [6, 7] provides the additional relationship

$$N_e = \sum_{n'}^{\dagger} f_{ns,n'p}, \tag{5}$$

where N_e is the number of active electrons.

For ions with ns and ns^2 ground states, the sum in equation (5) is characteristically dominated by the intrashell $\Delta n = 0$ transition. This results from the strong cancellation effects that affect line strength factors for $\Delta n \neq 0$ transitions, but do not occur for the $\Delta n = 0$ transition [8]. Since the lowest resonance transition is unbranched, its oscillator strength can be specified directly from lifetime measurements using equation (3). The f-sum rule provides a value for the remaining summed oscillator strength, and the second resonance level $ns(n+1)p$ $^1P_1^o$ provides a lower bound to subsequent excitation energies. This yields a bracketing inequality [9]

$$\frac{f_{ns,np}}{E_{ns,np}^2} \leqslant \alpha_d \leqslant \frac{f_{ns,np}}{E_{ns,np}^2} + \frac{N_e - f_{ns,np}}{E_{ns,(n+1)p}^2}. \tag{6}$$

If the width of the bracketing is small, then a reasonable estimate for the value of α_d can be obtained by taking the midpoint of the bracket

$$\alpha_d = \frac{f_{ns,np}}{E_{ns,np}^2} + \frac{N_e - f_{ns,np}}{2E_{ns,(n+1)p}^2}, \tag{7}$$

with an uncertainty given by the halfwidth of the bracket

$$\Delta\alpha_d = \frac{N_e - f_{ns,np}}{2E_{ns,(n+1)p}^2}. \tag{8}$$

This can be combined with the experimental uncertainties in the lifetime measurement to specify the total uncertainty in the determination.

Recent improvements in the accuracy of spectroscopic measurements now permit this procedure to be inverted [3], so that experimental results for α_d are used to specify values and uncertainty limits for $f_{ns,np}$ and τ_{np}. This can be accomplished by solving equation (7) for $f_{ns,np}$

$$f_{ns,np} = \frac{2\alpha_d E_{ns,(n+1)p}^2 - N_e}{2E_{ns,(n+1)p}^2/E_{ns,np}^2 - 1}. \tag{9}$$

Differentiating equation (9) and inserting equation (8), the bracketing uncertainty is

$$\Delta f_{ns,np} = \frac{N_e - f_{ns,np}}{2E_{ns,(n+1)p}^2/E_{ns,np}^2 - 1}. \tag{10}$$

In addition to adiabatic correlations such as α_d, a similar relationship connects $f_{ns,np}$ to the lowest order non-adiabatic correlation β [10], which is a measure of the inability of the core to instantaneously follow the motion of the outer electron. It is defined (in au)

$$\beta = \frac{1}{2}\sum_{n'}^{\dagger} \frac{f_{ns,n'p}}{E_{ns,n'p}^3}. \tag{11}$$

By the same considerations, β has the bracketing inequality

$$\frac{f_{ns,np}}{E_{ns,np}^3} \leqslant 2\beta \leqslant \frac{f_{ns,np}}{E_{ns,np}^3} + \frac{N_e - f_{ns,np}}{E_{ns,(n+1)p}^3}. \tag{12}$$

The central value is

$$\beta = \frac{f_{ns,np}}{2E_{ns,np}^3} + \frac{N_e - f_{ns,np}}{4E_{ns,(n+1)p}^3} \tag{13}$$

and the halfwidth is

$$\Delta\beta = \frac{N_e - f_{ns,np}}{4E_{ns,(n+1)p}^3}. \tag{14}$$

If the value of $f_{ns,np}$ can be specified by a measurement either of τ_{np} or of α_d, these expressions can be used to prescribe β.

2.2. Core contributions to N_e

The quantity N_e can be expected to be close to two, the number of out-of-shell ns^2 electrons in the ground state. However, there could be small additional contributions from the closed inner core. The Ne-, Ni-, Pd- and Pt-like ionic cores are, however, relatively rigid (cf [11] for calculations of α_d for the Ne and Ni sequences). To account for the possibility of an inner core contribution to the oscillator strength, let

$$N_e = 2 + \Delta N_e, \tag{15}$$

where ΔN_e is a small fraction. If $E_{ns,(n+1)p} \gg E_{ns,np}$ the bracketing widths will be small, and the results will be

Table 1. Lifetimes and BF for Ba II.

Transition	τ(ns)	BF(%)[a]	f	E(au)[b]
6s ^{2}S$_{1/2}$−6p ^{2}P$_{1/2}$	7.92(8)[c]	26.7	0.3380(34)	0.092 318
6s ^{2}S$_{1/2}$−6p ^{2}P$_{3/2}$	6.312(20)[d]	25.7	0.7370(23)	0.100 023
6s ^{2}S$_{1/2}$−7p ^{2}P$_{1/2}$				0.255 036

[a]Guet and Johnson [15].
[b]NIST [16].
[c]Kuske *et al* [13].
[d]Andrä [14].

insensitive to the value of ΔN_e. The effect of the assumed core contribution on the computations can be determined through controlled variation of the quantity ΔN_e.

An experimental estimate of ΔN_e could be obtained if a precision spectroscopic determination of α_d could be combined with a precision time-resolved measurement of τ_{np} for the same ion. The lifetime can be converted to the oscillator strength $f_{ns,np}$ using equation (3), and equation (7) can be solved for N_e to yield

$$N_e = f_{ns,np} + 2E_{ns,(n+1)p}^2 \left[\alpha_d - \frac{f_{ns,np}}{E_{ns,np}^2} \right]. \tag{16}$$

This expression can also be used to propagate the uncertainties in α_d and in τ_{np}, which can then be combined in quadrature. Once the value of N_e has been determined, it can be inserted into equations (13) and (14) to specify β.

2.2.1. Application to Ba$^+$. The Ba II ion provides an ideal test of this approach, since high precision data exist for both α_d and the lifetimes. This system has only one out-of-shell electron, and thus consists of doublets instead of singlets and triplets. Correspondingly, slight modifications must be made in the equations developed above to account for the fine structure of the lowest resonance transitions.

A high precision measurement of the polarizability of Ba II has been made [12] using laser resonant excitation Stark ionization spectroscopy (RESIS). This yielded a value α_d(Ba II) $= 123.88(5)a_0^3$. The lifetimes of the 6p ^{2}P$_{1/2}$ and 6p ^{2}P$_{3/2}$ levels have been measured to be $\tau_{6p1} = 7.92(8)$ ns [13] and $\tau_{6p3} = 6.312(20)$ ns [14]. In this system, the decays of the 6p levels are branched both to the 6s ground state and to the low-lying 5d levels. Thus conversion of the measured lifetimes to line strengths requires knowledge of the branching fractions (BF). Relativistic many-body perturbation theory calculations have been reported [15] for both the lifetimes and BF of these levels. For the absolute lifetime calculations, the agreement with experiment is at the 2% level. It is reasonable to assume that the relative calculations for the BF will be of even higher accuracy. The input data and the reduction of these lifetimes to f-values are indicated in table 1.

In terms of doublet levels, the corresponding version of equation (16) becomes

$$N_e = f_{6s,6p1} + f_{6s,6p3} + 2E_{6s,7p1}^2 \left[\alpha_d - \frac{f_{6s,6p1}}{E_{6s,6p1}^2} - \frac{f_{6s,6p3}}{E_{6s,6p3}^2} \right]. \tag{17}$$

Substitution of the values from table 1 yields $N_e = 2.204$. While the $n = 6$ shell contains only one active electron, the

$n = 5$ portion of the core has the configuration $5s^2 5p^6$. This result indicates that the core contributes slightly more than one active electron to the f-sum.

Substitution of values into the corresponding equations for β

$$\beta = \frac{f_{6s,6p1}}{2E_{6s,6p1}^3} + \frac{f_{6s,6p3}}{2E_{6s,6p3}^3} + \frac{N_e - f_{6s,6p1} - f_{6s,6p3}}{4E_{6s,7p1}^3} \qquad (18)$$

and its halfwidth

$$\Delta\beta = \frac{N_e - f_{6s,6p1} - f_{6s,6p3}}{4E_{6s,7p1}^3} \qquad (19)$$

yields a value $\beta = 605(25)a_0^5$.

2.3. Intermediate coupling

The relationships developed in section 2 assumed a single configuration with pure LS coupling. Both of these assumptions can be investigated through analysis of the energy spacings of the levels of the $nsnp$ configuration. Intermediate coupling produces singlet–triplet mixing between the $^1P_1^o$ and $^3P_1^o$ levels of this configuration. This can be characterized by extracting the mixing amplitudes from the measured energies of the $nsnp$ $^3P_2^o$, $^3P_1^o$, $^3P_0^o$ and $^1P_1^o$ levels [17]. Since there are three intervals and only two amplitudes (corresponding to the exchange Slater and spin–orbit energies [5]), the system is overdetermined. The two normalized amplitudes can be expressed as a single mixing angle θ. A solution involving only two of the splittings (taking the average energy of the $J = 1$ levels) is given by

$$\cot(2\theta) = \pm\frac{1}{\sqrt{2}}\left[\frac{3(^3P_1^o + {}^1P_1^o - 2{}^3P_0^o)}{(^3P_2^o - {}^3P_0^o)} - 1\right] \qquad (20)$$

(here the energy levels are designated by their spectroscopic symbols).

If the mixing angle deduced from this formula correctly predicts the $^1P_1^o$–$^3P_1^o$ splitting, this provides confirmation of the single configuration assumption. The effects of intermediate coupling can also be included by correcting the transition array value for $S_{ns,np}$ to obtain the resonance ($^1S_0$–$^1P_1^o$) and intercombination ($^1S_0$–$^3P_1^o$) values as

$$S(\text{Res}) = S_{ns,np}\cos^2\theta; \qquad S(\text{Int}) = S_{ns,np}\sin^2\theta. \qquad (21)$$

For line strengths $S(\text{Res})$ and $S(\text{Int})$ deduced from measured lifetimes, perturbations will generally cause the values of $S_{ns,np}$ for the two transitions to differ slightly. Thus, it is convenient to define two independent reduced line strengths

$$S_r(\text{Res}) \equiv S(\text{Res})/\cos^2\theta; \qquad S_r(\text{Int}) \equiv S(\text{Int})/\sin^2\theta, \qquad (22)$$

that can be displayed on the same plot. In this study, we are concerned only with the resonance transition.

In cases where singlet–triplet mixing is significant, the ground state oscillator strength is channeled through both the nominally labeled $^1P_1^o$ and $^3P_1^o$ levels. Since the triplet level lies below the singlet level, this is not accounted for in the energy denominator of the portion of the inequality utilizing the f-sum rule. Assuming that $S_{ns,np}$ is the same for both

of these levels, and noting the energy dependence of $f_{ns,np}$ in equation (2), correction factors can be constructed for the lower limits of both α_d and β as

$$\alpha_d \geqslant \frac{f_{ns,np}}{E_{ns,np}^2}\left[\cos^2\theta + \sin^2\theta\left(\frac{^1P_1^o}{^3P_1^o}\right)\right] \qquad (23)$$

and

$$\beta \geqslant \frac{f_{ns,np}}{E_{ns,np}^3}\left[\cos^2\theta + \sin^2\theta\left(\frac{^1P_1^o}{^3P_1^o}\right)^2\right], \qquad (24)$$

where ($^1P_1^o$/$^3P_1^o$) is the ratio of the singlet-to-triplet excitation energies. Since singlet–triplet mixing only redistributes the oscillator strength and does not alter the number of active electrons, it (unlike core excitation corrections) is included in the $N_e = 2$ f-sum rule.

3. Lifetimes deduced from measured dipole polarizabilities

There are several ions in these sequences for which dipole polarizability measurements have been reported. Through the use of equation (9), values for the lifetimes can be deduced. This approach is particularly valuable in cases in which direct measurement of the lifetime is strongly affected by cascading and blending.

Lifetime measurements in multiply-ionized systems are most commonly obtained by fast ion beam excitation achieved through traversal of a thin foil. Since this excitation method is non-selective, it produces multiexponential decay curves. This can be challenging to curve fitting methods in cases where the primary and one or more cascades have similar lifetimes. In such cases, the ANDC method [4] can be utilized. This method incorporates measured decay curves of the dominant cascades into the analysis of the primary in a correlated manner that effectively eliminates cascade effects.

3.1. Lifetime deduced from measured α_d for Si III

For Si III in the Mg sequence, a high precision measurement of α_d has been made [18], again using the RESIS technique. This yielded the value $\alpha_d(\text{SiIII}) = 11.666(4) \, a_0^3$.

For this ion, the measurement of the 3s3p $^1P_1^o$ lifetime is complicated by an unfortunate blend of the wavelengths [16] of the primary transition with its direct and indirect cascades, as well as by similar values for the primary and cascade lifetimes as predicted theoretically [19].

It can be seen from table 2 that the wavelengths of the primary 3s² $^1S_0$–3s3p $^1P_1^o$ transition and the direct cascade 3s3p $^1P_1^o$–3s3d $^1D_2$ both have wavelengths 1206.5 Å. Moreover, there are blends with the transitions 3p² $^1D_2$–3p3d $^1D_2^o$ at 1207.52 Å and 3p² $^1D_2$–3s4f $^1F_3^o$ at 1210.46 Å. (Here the upper levels 3p3d $^1D_2^o$ and 3s4f $^1F_3^o$ also act as indirect cascades through the 3s3d $^1D_2$ and 3p² $^1D_2$ levels.) Because of the Doppler broadening inherent in fast ion beam detection methods, it is virtually impossible to resolve these blends.

Measured lifetimes obtained from multiexponential curve fitting of the 3s3p $^1P_1^o$ decay have been reported as 0.40(10) [20] and 0.41(9) ns [21]. From table 2, it can be seen that theoretical calculations [19] predict a very similar lifetime of 0.44 ns for the direct cascade from 3p² $^1S_0$. Moreover, the

Table 2. Wavelengths and lifetimes of the primary and cascade transitions for ANDC analysis of ions in the Mg sequence.

Transition	Si III		P IV	
	λ(Å)	τ(ns)	λ(Å)	τ(ns)
$3s\ ^2\ ^1S_0 - 3s3p\ ^1P_1^o$	1206.5	0.407[a]	950.7	0.292[a]
$3s3p\ ^1P_1^o - 3p^2\ ^1S_0$	1417.2	0.44[b]	1118.6	0.33[b]
″ $-3s4s\ ^1S_0$	1312.6	1.11[b]	776.4	0.33[b]
″ $-3p^2\ ^1D_2$	2541.8	33[b]	1888.5	9.9[b]
″ $-3s3d\ ^1D_2$	1206.5	0.22[b]	877.5	0.12[b]

[a]Deduced from α_d.
[b]Theoretical estimate [19].

indirect cascades through $3p^2\ ^1D_2$ from the $3p3d\ ^1D_2^o$ and $3s4f$ $^1F_3^o$ levels are predicted [19] to be 0.43 and 0.61 ns.

　　Thus, because of congruences between cascade and primary lifetimes it is impossible to reliably extract the primary lifetime by multiexponential decay curve fitting. Because of blending between the wavelengths of the primary and cascade decay curves, it is also impossible to apply the ANDC method [4] to this system to account for the cascading. Since the spectral region and level system are not well suited to methods such as selective excitation by lasers, we must conclude that the lifetime of the $3s3p\ ^1P_1^o$ level in Si III cannot be measured with confidence using existing decay curve methods. Fortunately, the high precision measurement of α_d provides an alternative for determining τ_{3p} that is not affected by chance blending or cascade lifetime similarities.

　　Using equations (9) and (10), the measured value $\alpha_d = 11.666a_0^3$ yields $f_{3s,3p} = 1.610(61)$. The small uncertainty in the measurement of α_d is clearly negligible compared to the bracketing uncertainty. Using equation (3), the lifetime is deduced to be $\tau_{3p} = 0.407(15)$ ns. The results are summarized in table 3.

3.2. Lifetime deduced from measured α_d for P IV

A spectroscopic investigation of P III using vacuum sliding spark excitation has been reported [23]. This study yielded the value $\alpha_d(P\ IV) = 6.312a_0^3$, based on the (6–9) h ^{2}H levels in P III. No uncertainties were quoted, but a propagation of quoted wavelength tolerances and an examination of variances in our own weighted least squares fit to these data indicated a minimum uncertainty of $\pm 0.01a_0^3$.

　　For the $3s3p\ ^1P_1^o$ level in P IV, two lifetime measurements using multiexponential curve fitting yielded conflicting results $\tau_{3p} = 0.22(2)$ [24] and 0.35(2) ns [25]. It can be seen from table 2 that the direct cascades from $3p^2\ ^1S_0$ and $3s4s\ ^1S_0$ are both theoretically predicted [19] to have a lifetime of 0.33 ns, very close to one of the measurements reported. The possible effect of these cascades on the reliability of multiexponential fitting methods motivates the use of the ANDC method [4] for a joint analysis of these decay curves.

　　In order to resolve this discrepancy, we undertook fast ion beam measurements of the primary and cascade decay curves for an ANDC analysis. These measurements are described in section 4, and yielded a result that confirms the analysis described below.

　　The measured value of α_d provides an independent means of determining this lifetime. Although the precision

of this value of α_d is substantially less than that obtained by the RESIS method, its accuracy in predicting τ_{3p} remains competitive with direct lifetime measurements. Using equations (9) and (10), the measured value $\alpha_d(P\ IV) = 6.312a_0^3$ yields $f_{3s,3p} = 1.391(65)$. Using equation (3), the lifetime is deduced to be $\tau_{3p} = 0.292(14)$ ns. The results are summarized in table 3.

3.3. Lifetimes deduced from measured α_d for Kr VII

This method has recently been applied [3] to a precision measurement [26] of α_d in Kr VII, again using the RESIS method. The measured result was $\alpha_d = 2.69(4)a_0^3$, and using this method the values $\tau_{4p} = 0.096(3)$ ns and $\beta = 1.71(3)a_0^5$ were deduced. This lifetime determination is consistent with a fast ion beam measurement [27] and with theoretical estimates [28, 29], but represents a significant improvement in precision. The results are summarized in table 3.

3.4. Lifetimes deduced from measured α_d for Pb III

In a spectroscopic study of g and h states in Pb II, Ross *et al* [30] used the polarization model to obtain a value for the dipole polarizability of Pb III at $\alpha_d = 13.38a_0^3$ (1.982 Å^3).

　　This value yields an upper limit $f_{6s,6p} \leqslant \alpha_d E_{6s,6p}^2 = 2.525$, which exceeds the value for N_e used in the f-sum rule, and leads to non-physical results in equation (9). If we assume that the intrashell transition dominates the f-sum, the value is $f_{6s,6p} \approx N_e \approx 2.5$. The lifetime corresponding to this lifetime is $\tau_{6p} \approx 0.2$. Thus, the values for neither $f_{6s,6p}$ nor τ_{6p} deduced from this measurement of α_d is consistent with isoelectronic trends [31]. A reexamination of this measurement of α_d is recommended.

　　In view of these discrepancies, the value of τ_{6p} obtained from fast ion beam measurements [31] is adopted and the value of α_d of [30] is rejected in all subsequent calculations herein.

4. Fast ion beam lifetime measurements in P IV

Lifetime measurements were performed in the University of Toledo Heavy Ion Accelerator Laboratory. The facilities, including a Danfysik 300 kV accelerator and an on-line data analysis system have been described earlier [32, 33].

　　Singly charged P$^+$ ions of energies 170 and 240 keV were directed through thin (2.1–2.4 μg cm^{-2}) carbon foils. Corrections were made for energy loss in the foil (typically 5 keV). The emitted radiation was dispersed with an Acton 1-m normal incidence vacuum monochromator. Depending on the wavelength range, detection was achieved either with a channel electron multiplier and a 2400 lines mm^{-1} grating (blazed at 800 Å), or a Hamamatsu 7154 photomultiplier tube and a 1200 lines mm^{-1} grating (blazed at 1500 Å). Decay curves were measured by recording the emitted intensity of a given spectral line as a function of distance from the foil, achieved by translating the foil relative to the point of observation. The decay curves were first analyzed using the multiexponential fitting program DISCRETE [34], and then by the ANDC method [4], which corrects for cascading in a rigorous way.

Table 3. Specification of lifetimes from measured dipole polarizabilities. Uncertainties are in parentheses, energies are from [16].

n	Ion	$\alpha_d(a_0^3)$	$f_{ns,np}$	τ_{np}(ns)		
				From α_d	Measured	Theory
3	Si III	11.666(4)[a]	1.610(61)	0.407(15)	0.40(10)[b], 0.41(9)[c]	0.408[d], 0.429[e]
3	P IV	6.312[f]	1.391(65)	0.292(14)	0.22(2)[g], 0.35(2)[h], 0.287[i]	0.276[d], 0.295[e]
4	Kr VII	2.69(5)[j]	1.60(4)	0.096(3)[k]	0.101(10)[l]	0.0991[m], 0.0953[n]
6	Pb III	13.38[o]	≈2.5	≈0.2	0.380(21)[p]	0.360[p]

[a]Komara *et al* [18]; [b]Berry *et al* [20]; [c]Livingston *et al* [21]; [d]Tachiev and Fischer [19];
[e]Safronova *et al* [22]; [f]Magnusson and Zetterberg [23]; [g]Curtis *et al* [24]; [h]Livingston *et al* [25];
[i]This work; [j]Lundeen and Fahrenbach [26]; [k]Curtis [3]; [l]Pinnington *et al* [27];
[m]Liu *et al* [28]; [n]Chou *et al* [29]; [o]Ross *et al* [30]; and [p]Curtis *et al* [31].

The cascade scheme is indicated in table 2. Measurements were made of the decay curves for the primary transition from 3s3p $^1P_1^o$ at 950.655 Å, the cascades from the 3p^2 and 3s4s $^1S_0$ levels at 1118.6 and 776.4 Å, and the cascades from the 3p^2 and 3s3d $^1D_2$ levels at 1888.5 and 877.5 Å. Unfortunately the decay curve of the 3p^2 $^1S_0$ was obscured by a blend with the strong 3s $^2S_{1/2}$–3p $^2P_{3/2}^o$ resonance transition in P V at 1118.551 Å.

Attempts were made to resolve this blend by variation of the beam energy, and by comparing the exponential content on opposing wings of the line-width. (If the individual contributions of the blended lines vary over the profile of the line, the ANDC method can be extended to resolve the blend [35, 36].) However, the P V line was too strong to be deblended by either of these methods.

Multiexponential curve fits yielded the following results for the primary and the two unblended cascades: the 950 Å primary yielded two exponentials with lifetimes 0.35 and 9.5 ns; the 776.4 Å cascade yielded two exponentials with lifetimes 0.49 and 5.7 ns; the 1888.5 Å cascade yielded a single exponential with a lifetime 8.1 ns; and the 877.5 Å cascade yielded two exponentials with lifetimes 0.2 and 4.4 ns. The 1118.6 Å decay curve yielded a lifetime corresponding to the P V line with which it was blended. Theoretical estimates for the lifetimes of the upper levels of these decays are given in table 2.

An ANDC analysis was carried out on the primary transition at 950 Å and the cascades at 1888.5, 877.5 and 776.4 Å, but omitting the blended line at 1118.6 Å. The ANDC analysis rejected the inclusion of the 877.5 Å line, but gave a good result with the inclusion of the 1118.6 and 774.6 Å cascades.

The rejection of the 3s3d $^1D_2$–3s4f $^1F_3^o$ cascade transition at 877.5 Å by the ANDC mechanism was initially puzzling, since it is a member of the 3s^2–3s3p–3s3d–3s4f ... series. In the Na sequence, the 3s–3p–3d–4f ... series forms an unbranched link to the yrast chain of circular orbit transitions, and dominates the repopulation of the lowest resonance transition. However, Hutton *et al* [37] have pointed out a significant difference for Mg-like systems.

In the Mg sequence cascading is altered by the existence of the 3p^2 $^1D_2$ level, which lies well below the 3s3p $^1D_2$ level in energy. Although the 3p^2–3s4f transition is nominally a two-electron jump, there is heavy configuration mixing between the 3s3d $^1D_2$ and 3p^2 $^1D_2$ levels, and the theoretical line strengths [19] of the 3s3d $^1D_2$–3s4f $^1F_3^o$ and 3p^2 $^1D_2$–3s4f

$^1F_3^o$ transitions are of similar magnitude. Thus the wavelength-cubed factor (≈10) causes the repopulation to branch strongly through the 3p^2 channel and to effectively bypass the 3s3d channel.

This demonstrates the power of ANDC analysis to confirm the correlations between cascade-coupled decay curves. It should be noted that the ANDC method has been applied to other members of this sequence [35, 37–41], and the relative contributions of the cascades from 3s3d $^1D_2$ and 3p^2 $^1D_2$ could provide a probe of this configuration mixing.

The ANDC method involves the consideration of the instantaneous population equation, expressed in terms of the measured decay curves $I_k(t)$ and of the detection efficiencies ζ_k of the cascades relative to the primary transition. For this system, this equation can be written

$$\mathrm{d}I_1/\mathrm{d}t = \zeta_2 I_2(t) + \zeta_3 I_3(t) - I_1(t)/\tau_1, \qquad (25)$$

where the indices 1, 2 and 3 denote the 950, 774.5 and 1118.6 Å transitions. This can be rewritten in the form

$$-\frac{\mathrm{d}}{\mathrm{d}t}[\ln I_1] = \frac{1}{\tau_1} - \zeta_2 \left[\frac{I_2(t) + eI_3(t)}{I_1(t)} \right], \qquad (26)$$

where $e \equiv \zeta_3/\zeta_2$. The quantities τ_1, ζ_2 and ζ_3 are then adjusted as fitting parameters to the measured values for the various decay curves I_k. The numerical logarithmic derivative can be conveniently performed using a moving polynomial fit [42].

An ANDC plot is shown in figure 1. If the method is successful, this plot is linear with the reciprocal lifetime specified by the intercept on the ordinate. The intercept obtained here was 3.483 ns^{-1} corresponding to a lifetime $\tau = 0.287$ ns, in excellent agreement with the result obtained from the polarizability data. There is some slight irregularity in the ANDC plot, presumably owing to the omission of the blended cascade. Thus the precision of the polarizability determination is probably higher than the ANDC measurement, which nonetheless provides a persuasive confirmation.

5. Predictive systematization of line strength data for the ns^2–$nsnp$ isoelectronic sequences

There is extensive empirical evidence [31, 43–45] indicating that ions with two out-of-shell electrons exhibit a nearly linear isoelectronic variation when the multiplet line strength $S_{ns,np}$ is quadratically scaled with nuclear charge and plotted against a suitably chosen reciprocal screened charge.

6
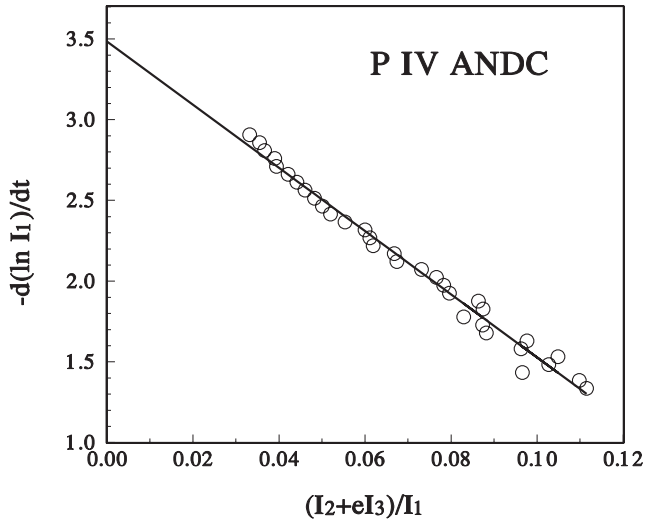
Figure 1. ANDC analysis for P IV. The intercept yields a reciprocal lifetime 3.483 ns^{-1}, corresponding to $\tau_1 = 0.287$ ns.

In these systems, it is possible to account for the effects of intermediate coupling using the singlet–triplet mixing angles obtained from equation (20). Here, we are concerned only with the resonance line strengths S(Res). First, empirical line strength factors S(Res) are deduced from measured lifetimes using equations (2) and (3). These values are then converted to effective reduced multiplet values S_r(Res) using equations (21). The quantity S_r can then be isoelectronically parametrized using

$$Z^2 S_r = S_H + B/(Z - C). \qquad (27)$$

It has been demonstrated [46] that for large Z the trend approaches the hydrogenic limit S_H, given by

$$S_H = \tfrac{9}{2} n^2 (n^2 - 1). \qquad (28)$$

Thus, for $n = 3, 4, 5$ and 6, $S_H = 324, 1080, 2700$ and 5670.

Figure 2 shows a plot of $Z^2 \sim S_r$ versus $1/(Z - C)$ for the resonance transitions in each of these four sequences. Open circles denote values deduced from τ_{np} measurements. Filled circles denote values deduced from α_d measurements. Filled diamonds indicate the high-Z hydrogenic values S_H.

A weighted least-squares fit can be made to the measured values for S_r. This can be interpolated to obtain values for all members of the sequence, and used to specify the corresponding values for $f_{ns,np}$ and α_d.

6. Determination of α_d and β from lifetime data

6.1. Tabulations of results

We have used the lifetime database to compute α_d for members of the homologous Mg, Zn, Cd and Hg isoelectronic
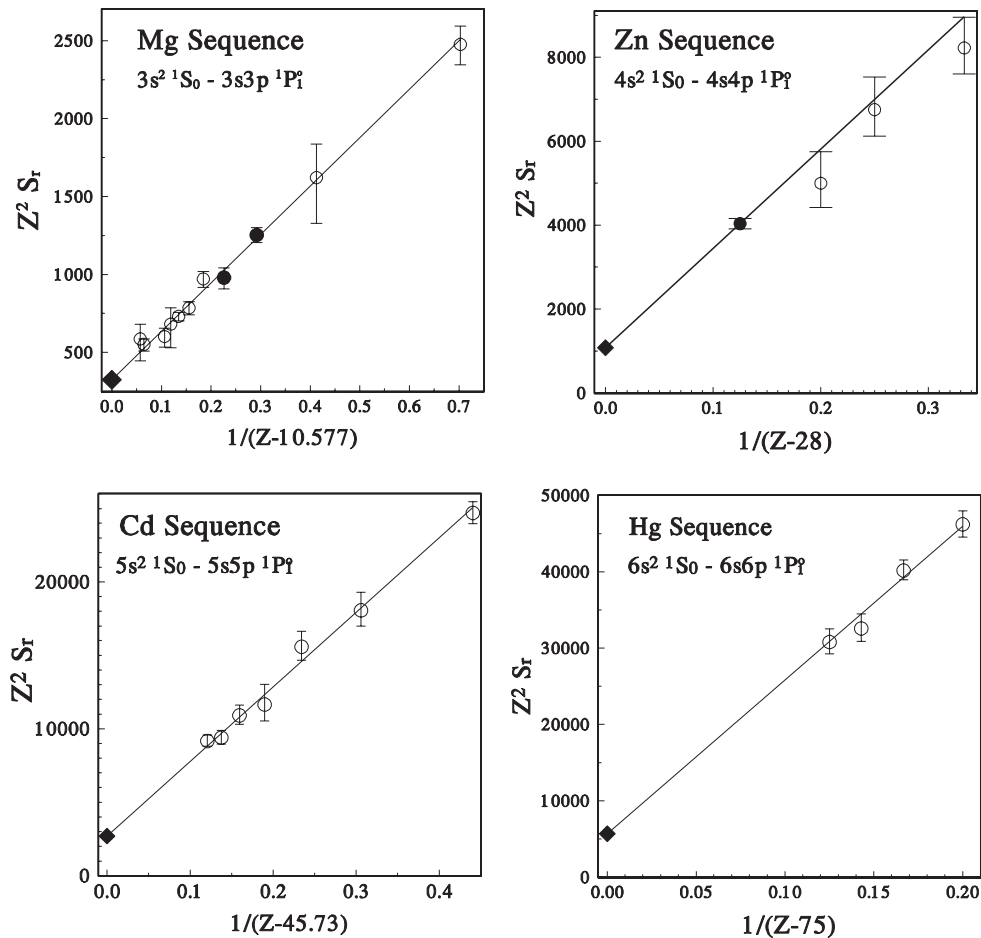
Figure 2. Isoelectronic interpolation of the reduced line strengths for the homologous $ns^2\ ^1S_0 - nsnp\ ^1P_1^o$ transitions. Open circles denote values deduced from τ_{np} measurements. Filled circles denote values deduced from α_d measurements. Filled diamonds indicate the high-Z hydrogenic asymptotes.

Table 4. Analysis for the Mg isoelectronic sequence. Energies are from [16]. Brackets denote values obtained from isoelectronic interpolation of line strengths as described in [43].

Z	Ion	$E_{3s,3p}$(au)	$E_{3s,4p}$(au)	τ_{3p}(ns)	$f_{3s,3p}$	$\alpha_d(a_0^3)$	$\beta(a_0^5)$
12	Mg	0.159 705	0.224 840	2.0(1)[a]	1.830	74.4(27)	230.6(59)
13	Al	0.272 706	0.487 166	0.72(11)[b]	1.744	24.20(75)	43.8(8)
14	Si	0.377 649	0.804 135	0.407(15)[c]	1.610	11.666(4)	15.18(24)
15	P	0.479 283	1.173 360	0.292(14)[c]	1.391	6.312(10)	6.43(11)
16	S	0.579 341	1.592 596	0.19(1)[d]	1.464	4.49(13)	3.80(4)
17	Cl	0.678 653	2.085 826	0.165(9)[e]	1.229	2.77(10)	1.99(2)
18	Ar	0.777 866	2.596 186	0.132(5)[f]	1.169	2.00(7)	1.26(1)
19	K	0.877 263	3.168 366	0.11(2)[g]	1.103	1.48(5)	0.825(8)
20	Ca	0.977 252	3.792 302	0.10(1)[h]	0.978	1.06(4)	0.530(5)
21	Sc	1.078 074	4.467 961	[0.078]	1.030	0.914(27)	0.415(3)
22	Ti	1.179 963	5.193 858	[0.068]	0.986	0.730(21)	0.303(2)
23	V	1.283 187	5.971 077	[0.060]	0.945	0.591(16)	0.2258(14)
24	Cr	1.387 992	6.802 244	[0.053]	0.914	0.488(13)	0.1727(1)
25	Mn	1.494 669	7.680 159	[0.048]	0.871	0.401(10)	0.1319(7)
26	Fe	1.603 424	8.611 337	0.042(3)[i]	0.865	0.346(8)	0.1062(5)
27	Co	1.714 654	9.841 775	[0.039]	0.814	0.285(7)	0.0820(3)
28	Ni	1.828 466	10.631 750	0.031(6)[j]	0.901	0.276(5)	0.0749(3)

[a]Liljeby *et al* [47]; [b]Kernahan *et al* [48]; [c]This work. [d]Reistad *et al* [35];
[e]Engström *et al* [38]; [f]Reistad *et al* [39]; [g]Biémont *et al* [49]; [h]Träbert *et al* [40];
[i]Hutton *et al* [41]; [j]Hutton *et al* [37].

Table 5. Analysis for the Zn isoelectronic sequence. Energies are from [16]. Brackets denote values obtained from isoelectronic interpolation of line strengths as described in [44].

Z	Ion	$E_{4s,4p}$(au)	$E_{4s,5p}$(au)	τ_{4p}(ns)	$f_{4s,4p}$	$\alpha_d(a_0^3)$	$\beta(a_0^5)$
30	Zn	0.212 988	0.286 641	1.33(7)[a]	1.548	37.5(34)	86.0(59)
31	Ga	0.322 139	0.549 267	0.49(4)[b]	1.836	18.14(44)	27.9(4)
32	Ge	0.418 603	0.839 724	0.29(3)[b]	1.837	10.68(19)	12.66(11)
33	As	0.510 410	1.157 491	0.23(3)[b]	1.558	6.19(20)	5.96(9)
34	Se	0.600 220	1.492 633	[0.16]	1.620	4.61(11)	3.80(4)
35	Br	0.689 132	1.865 496	[0.126]	1.560	3.37(8)	2.42(2)
36	Kr	0.778 382	2.267 324	0.096(3)[c]	1.598	2.70(5)	1.718(11)
37	Rb	0.867 986	2.690 311	[0.084]	1.468	2.00(4)	1.142(8)
38	Sr	0.958 553	3.157 864	[0.071]	1.429	1.597(33)	0.827(5)
39	Y	1.050 367	3.646 581	[0.061]	1.394	1.299(27)	0.615(4)
40	Zr	1.143 781	4.164 263	[0.052]	1.362	1.071(21)	0.466(3)
41	Nb	1.239 045	4.710 904	[0.046]	1.334	0.895(17)	0.361(2)
42	Mo	1.336 523	5.191 224	[0.040]	1.307	0.755(15)	0.2829(14)
43	Tc	1.436 289	5.891 082	[0.035]	1.282	0.644(12)	0.2262(10)
44	Ru	1.538 752	6.524 613	[0.031]	1.260	0.552(10)	0.1819(7)
45	Rh	1.644 053	7.187 109	[0.028]	1.238	0.477(8)	0.1477(6)
46	Pd	1.752 640	7.878 569	[0.025]	1.216	0.413(7)	0.1207(5)
47	Ag	1.864 776	8.598 994	[0.022]	1.199	0.361(6)	0.0997(4)

[a]Martinson *et al* [50]; [b]Andersen *et al* [51]; [c]Curtis [3].

sequences. The results are presented in tables 4–7. Energy level and lifetime data were drawn from [47]–[71].

Spectroscopic energy level source references are indicated in the table captions. Lifetime measurements are indicated with quoted uncertainties in parentheses, drawn from references as footnotes. Isoelectronic interpolations for lifetimes are also indicated, enclosed in brackets. In three cases, Si III, P IV and Kr VII, lifetime values were deduced from measurements of α_d. The lifetimes were first converted to oscillator strengths using equation (3). The energies and oscillator strengths were then used to compute α_d and $\Delta\alpha_d$ using equations (7) and (8) and to compute β and $\Delta\beta$ using equations (13) and (14). In the cases of Si III, P IV and Kr VII the calculation simply recovers the values of α_d from which the lifetimes were deduced. The uncertainties quoted in parentheses for α_d and β indicate only the bracketing uncertainties.

In cases where a lifetime measurement was made, the quoted measurement uncertainties should be propagated and added in quadrature with the bracketing uncertainties to obtain the total precision.

Fraga *et al* [72] have made calculations of static dipole polarizabilities for virtually all charge states of all elements using the Hartree–Fock relativistic (HFR) [73] approximation. These calculations give general qualitative agreement with our determinations for the Mg and Zn sequences, but they become increasingly larger than our values for the Cd and Hg sequences.

Biémont *et al* [74] have commented on this fact, noting that concerning the values of Fraga *et al*, 'It was verified that consideration of the parameters $\alpha_d = 22.33$ and $r_c = 2.39$ au of the Pb III ion leads to an overestimate of the polarization effects'. Indeed, the value $22.33 a_0^3$ predicted by

Table 6. Analysis for the Cd isoelectronic sequence. Energies are from [16] and [52]. Brackets denote values obtained from isoelectronic interpolation of line strengths as described in [45].

Z	Ion	$E_{5s,5p}$(au)	$E_{5s,6p}$(au)	τ_{5p}(ns)	$f_{5s,5p}$	$\alpha_d(a_0^3)$	$\beta(a_0^5)$
48	Cd	0.199 078	0.298 404	1.66(5)[a]	1.419	39.7(38)	96.5(64)
49	In	0.287 203	0.500 174	0.79(5)[b]	1.433	18.8(13)	31.7(13)
50	Sn	0.364 103	0.741 430	0.47(3)[c]	1.499	11.9(5)	16.0(4)
51	Sb	0.437 190	0.997 965	0.38(4)[d]	1.286	7.19(41)	8.0(2)
52	Te	0.508 979	1.269 863	0.269(16)[e]	1.350	5.50(23)	5.26(9)
53	I	0.580 587	1.556 909	0.220(11)[f]	1.288	4.04(17)	3.39(5)
54	Xe	0.652 745	1.858 096	0.165(7)[g]	1.328	3.28(11)	2.46(3)
55	Cs	0.725 947	2.169 508	[0.166]	1.067	2.17(11)	1.447(25)
56	Ba	0.800 598	2.512 372	[0.142]	1.028	1.73(11)	1.043(16)
57	La	0.877 008	2.846 534	[0.118]	1.027	1.44(6)	0.794(11)
58	Ce	0.955 477	3.218 386	[0.100]	1.023	1.21(5)	0.614(8)
59	Pr	1.013 557	3.599 236	[0.085]	1.072	1.12(4)	0.540(6)

[a]Lurio and Novick [53]; [b]Ansbacher *et al* [54]; [c]Pinnington *et al* [55]; [d]Pinnington *et al* [56]; [e]Weighted average of [57] and [58]; [f]Weighted average of [59] and [60]; [g]Weighted average of [57] and [61].

Table 7. Analysis for the Hg isoelectronic sequence Energies are from [62] and [31]. Brackets denote values obtained from isoelectronic interpolation of line strengths as described in [31]. Polarizabilites are given both in the *LS* coupling limit and with corrections for intermediate coupling.

Z	Ion	$E_{6s,6p}$(au)	$E_{6s,7p}$(au)	τ_{6p}(ns)	$f_{6s,6p}$	$\alpha_d(a_0^3)$	$\beta(a_0^5)$
80	Hg	0.246 356	0.325 018	1.34(3)[a]	1.148	23.6(45)	46.4(69)
81	Tl	0.344 732	0.557 600	0.59(4)[b]	1.332	12.7(12)	18.3(11)
82	Pb	0.434 402	0.807 298	0.380(21)[c]	1.302	7.8(6)	9.0(4)
83	Bi	0.522 165	1.056 673	0.243(13)[d]	1.409	5.7(3)	5.69(15)
84	Po	0.609 173	1.297 816	[0.176]	1.430	4.3(2)	3.74(8)
85	At	0.697 484	1.542 283	[0.133]	1.443	3.33(14)	2.58(4)
86	Rn	0.787 549	1.786 749	[0.104]	1.448	2.64(10)	1.85(3)
87	Fr	0.880 202	2.031 216	[0.0829]	1.454	2.15(8)	1.37(2)
88	Ra	0.975 903	2.275 683	[0.0671]	1.461	1.78(6)	1.043(14)
89	Ac	1.074 698	2.520 150	[0.0550]	1.470	1.49(5)	0.810(10)
90	Th	1.177 075	2.764 617	[0.0455]	1.481	1.26(4)	0.640(7)
91	Pa	1.283 438	3.009 084	[0.0380]	1.492	1.08(3)	0.513(6)
92	U	1.394 129	3.253 551	[0.0319]	1.506	0.94(3)	0.418(4)

[a]Weighted average of [63–68]; [b]Henderson and Curtis [69]; [c]Ansbacher *et al* [70]; [d]Ansbacher *et al* [71].

Fraga *et al* [72] compares unfavorably both with the value $13.38a_0^3$ deduced from spectroscopic data for Pb II by Ross *et al* [30], and with the value $7.5a_0^3$ deduced from measured lifetime data in table 7. As discussed in section 3.2, both of these larger values for α_d(Pb III) conflict with f-sum rules and experimental line strength trends. The predictions of α_d for the Au isoelectronic sequence are also much larger than recent empirical determinations for Au I–Bi V reported by Henderson *et al* [75].

6.2. Theoretical predictions for charge scaling

The width of the bracketing inequality (and hence the influence of its uncertainty) will be small if: $f_{ns,np}$ is large; $E_{ns,np}$ is small; and $E_{ns,(n+1)p}$ is close to the ionization limit. Some insights can be gained by considering isoelectronic scaling.

We denote by ζ the effective core charge seen by the jumping electron (the nuclear charge minus the number of electrons save one). In terms of this quantity Cowan [73] (pp 436–9) has summarized the approximate isoelectronic variation of oscillator strengths and energies. For intershell transitions, the expected scaling is

$$f_{ns,(n+1)p} \propto \text{constant}; \quad E_{ns,(n+1)p} \propto \zeta^2; \quad (\Delta n \neq 0), \quad (29)$$

whereas for intrashell transitions

$$f_{ns,np} \propto 1/\zeta; \quad E_{ns,np} \propto \zeta; \quad (\Delta n = 0). \quad (30)$$

For determining α_d, the quantities in equation (6) scale as

$$f_{ns,np}/E_{ns,np}^2 \propto 1/\zeta^3; \quad f_{ns,(n+1)p}/E_{ns,(n+1)p}^2 \propto 1/\zeta^4. \quad (31)$$

Thus, although the contribution of $f_{ns,np}$ to the total f-sum decreases relative to that of the intershell transitions with increasing ζ, the ratio of the bracketing width to the lower limit of α_d decreases as $1/\zeta$. (Notice that here the central value of α_d scales as the sum of a large $1/\zeta^3$ term and a small $1/\zeta^4$ term, in contrast to the hydrogenic value which, involving only intershell transitions, scales as $1/\zeta^4$.)

For determining β, the quantities in equation (11) scale as

$$f_{ns,np}/E_{ns,np}^3 \propto 1/\zeta^4; \quad f_{ns,(n+1)p}/E_{ns,(n+1)p}^3 \propto 1/\zeta^6, \quad (32)$$

so the ratio of the bracketing width to the lower limit of β decreases even faster, as $1/\zeta^2$. For α_d the relationship is more complicated, but for very large Z the bracketing and the upper limit scale together.

Table 8. Scaling.

Sequence	B_α	d_α	p_α	B_β	d_β	p_β
Mg	2427	2.43	3.18	1148	0.61	3.37
Zn	504.7	1.96	2.42	2545	1.74	3.40
Cd	548.0	2.04	2.38	2667	1.78	3.28
Hg	231.4	2.05	2.08	1509	2.09	3.15

6.3. Charge scaling of the results

The polarizability data in tables 4–7 were fitted to the charge scaling equations

$$\alpha_d = \frac{B_\alpha}{(\zeta + d_\alpha)^{p_\alpha}}; \qquad \beta = \frac{B_\beta}{(\zeta + d_\beta)^{p_\beta}}. \qquad (33)$$

The fitted values are listed in table 8.

7. Relativistic effects in the Hg sequence

Homologous comparisons of these four isoelectronic sequences reveal interesting trends. It can be seen from tables 4–7 that the oscillator strengths $f_{ns,np}$ decrease with increasing ionicity, consistent with the $\Delta n = 0$ scaling with $1/\zeta$ that was predicted in equation (30). However, table 7 reveals that for the Hg sequence the oscillator $f_{6s,6p}$ is nearly constant over the sequence, as would be expected for a $\Delta n \neq 0$ transition as predicted in equation (29). In all four sequences the $E_{ns,np}$ energy decreases with ζ as expected, so the difference in scaling resides in the line strength factor.

The origin of this behavior lies in significant relativistic corrections that affect Hg and its isoelectronic sequence [76, 77]. In earlier studies of the Cd [45] and Hg [31] sequences, multiconfiguration Dirac Hartree Fock (MCDHF) calculations showed that $6s^2$ and $6s6p$ remain lower than plunging levels from the 5f and 5g subshells for all ions through uranium. In contrast, for the Cd sequence, plunging levels from the 4f subshell perturb the 5s5p levels above $Z = 60$ and for $Z > 62$ the 4f levels replace $5s^2$ as the ground state. Moreover, whereas the mixing angle reduction could be accomplished using the Schrödinger formalism with LS coupling for the Mg, Zn and Cd sequences, MCDHF calculations for the Hg sequence indicated a significant difference between the Dirac transition matrices $\langle s_{1/2}|r|p_{1/2}\rangle$ and $\langle s_{1/2}|r|p_{3/2}\rangle$, requiring use of the Dirac formalism and jj coupling.

The reasons for these observations are closely related to the unusual fact that mercury is a liquid at ambient temperatures. The 6s electrons (and each s electron in the core) are drawn in because of relativistic effects at small r. It can be made plausible in terms of the Bohr orbit picture, since the speed of the 6s electron at periapsis is $v \approx Zc/137$ (for $Z = 80$, $v = 0.58c$). The increase in the relativistic mass causes the effective Bohr radius to shrink (although Zitterbewegung and the Darwin term decrease the effect somewhat). Moreover, the magnetic coupling of the two paired s electrons is enhanced by the predominance of jj coupling, since spin–own–orbit coupling to the nucleus dominates over spin–spin, orbit–orbit and spin–other–orbit coupling to other electrons. Thus mercury atoms and ions in the Hg sequence behave more like an inert gas than an alkaline earth.

It has been noted [76] that gold and mercury differ in melting points, densities, electrical conductivities, the ability to amalgamate with noble metals, etc, by greater factors than virtually any other pair of neighbors in the Periodic table. Similarly, Tl II is more stable than Tl I, Pb III is more stable than Pb II, and Bi IV is more stable than Bi III. Relativistic calculations have also explained the difference in color between gold and silver [77].

Only the first four members of the Hg sequence are radioactively stable, and measurements of the atomic structure properties of its radioactive members are lacking. However, the atomic properties of the radioactive members have applications in, e.g. modeling calculations of radiation transfer in astrophysical and controlled fusion plasmas. Thus semiempirical extrapolations can provide useful estimates for the ions in this sequence with $Z \geqslant 84$.

8. Conclusions

For atomic systems in which the ground state oscillator strength is dominantly concentrated in one low-lying resonance transition, the method described here provides a powerful means to interconnect measurements and predictions of the quantities α_d, β and τ. If a precision measurement of τ is available, α_d and β can be deduced. Alternatively, if a precision measurement of α_d is available, τ and β can be deduced. Moreover, screening parametrizations of line strength data permit isoelectronic interpolation of a few precise measurements to obtain estimates of these quantities for the entire sequence. The Mg, Zn, Cd and Hg sequences satisfy these criteria very well, and the results presented here provide an extensive database spanning both homologous and isoelectronic sequences.

References

[1] B Edlén B 1964 Atomic Spectra *Handbuch der Physik XXVII* ed Flügge S (Berlin: Springer) section 20 pp 80–220
[2] Dalgarno A and Kingston A E 1959 *Proc. Phys. Soc.* **74** 455–64
[3] Curtis L J 2007 *J. Phys. B: At. Mol. Opt. Phys.* **40** 3173–80
[4] Curtis L J, Berry H G and Bromander J 1971 *Phys. Lett.* **34A** 169–70
[5] Curtis L J 2003 *Atomic Structure and Lifetimes: A Conceptual Approach* (Cambridge: Cambridge University Press)
[6] Kuhn W 1925 *Z. Phys.* **33** 408–12
[7] Reiche F and Thomas W 1925 *Z. Phys.* **34** 510–25
[8] Curtis L J 1991 *Can. J. Phys.* **69** 668–70
[9] Miller T M and Bederson B 1977 *Adv. At. Mol. Phys.* **13** 1–55
[10] Kleinman C J, Hahn Y and Spruch L 1968 *Phys. Rev.* **165** 53–62
[11] Johnson W R, Kolb D and Huang K-N 1983 *At. Data Nucl. Data Tables* **28** 333–40
[12] Snow E and Lundeen S R 2007 *Phys. Rev.* A **76** 052505

[13] Kuske P, Kirchner N, Wittman W, Andrä H J and Kaiser D 1978 *Phys. Lett.* A **64** 377

[14] Andrä H J 1976 *Beam-Foil Spectroscopy* vol 2 ed I A Sellin and D J Pegg (New York: Plenum) p 835

[15] Guet C and Johnson W R 1991 *Phys. Rev.* A **44** 1531–5

[16] NIST Physical Reference Data Online at http://physics.nist.gov/PhysRefData/contents.html

[17] Curtis L J 1989 *Phys. Rev.* A **40** 6958–68

[18] Komara R A, Gearba M A, Fehrenbach C W and Lundeen S R 2005 *J. Phys. B: At. Mol. Opt. Phys.* **38** S87–S95

[19] Tachiev G and Froese Fischer C 2002 The MCHF/MCDHF Collection http://atoms.vuse.vanderbilt.edu

[20] Berry H G, Bromander J, Curtis L J and Buchta R 1971 *Phys. Scr.* **3** 125–32

[21] Livingston A E, Dumont P D, Baudinet-Robinet Y, Garnir H P, Biémont E and Grevesse N 1976 *Beam-Foil Spectroscopy* ed I A Sellin and D J Pegg (New York: Plenum) pp 339–46

[22] Safronova U, Johnson W R and Berry H G 2000 *Phys. Rev.* A **61** 052503

[23] Magnusson C E and Zetterberg P O 1977 *Phys. Scr.* **15** 237–50

[24] Curtis L J, Martinson I and Buchta R 1971 *Phys. Scr.* **3** 197–202

[25] Livingston A E, Kernahan J A, Irwin D J G and Pinnington E H 1975 *Phys. Scr.* **12** 223–9

[26] Lundeen S R and Fahrenbach C W 2007 *Phys. Rev.* A **75** 032523

[27] Pinnington E H, Ansbacher W and Kernahan J A 1984 *J. Opt. Soc. Am.* B **1** 30–3

[28] Liu L, Hutton R, Zou Y, Andersson M and Brage T 2006 *J. Phys. B: At. Mol. Opt. Phys.* **39** 3147–58

[29] Chou H-S, Chi H-C and Huang K-N 1994 *Phys. Rev.* A **49** 2394–8

[30] Ross C B, Wood D R and Scholl P S 1976 *J. Opt. Soc. Am.* **66** 36–9

[31] Curtis L J, Irving R E, Henderson M, Matulioniene R, Froese Fischer C and Pinnington E 2001 *Phys. Rev.* A **63** 042502 1–7

[32] Haar R R, Beideck D J, Curtis L J, Kvale T J, Sen A, Schectman R M and Stevens H 1993 *Nucl. Instrum. Methods Phys. Res.* **79** 746–8

[33] Haar R R and Curtis L J 1994 *Nucl. Instrum. Methods Phys. Res.* **79** 782–4

[34] Provencher S W 1976 *J. Chem. Phys* **64** 2772–7

[35] Reistad N, Jupén C, Huldt S, Engström L and Martinson I 1985 *Phys. Scr.* **32** 164–8

[36] Curtis L J 1971 *Proc. 2nd European Conf. on Beam Foil Spectroscopy Lyon, France* ed Dufay M

[37] Hutton R, Reistad N, Martinson I, Träbert E, Heckmann P H, Blanke J H, Hellmann H M and Hucke R 1987 *Phys. Scr.* **35** 300–2

[38] Engström L, Bengtsson P, Jupén C, Livingston A E and Martinson I 1995 *Phys. Rev.* A **51** 179–84

[39] Reistad N, Engström L and Berry H G 1986 *Phys. Scr.* **34** 158–63

[40] Träbert E, Pinnington E H, Kernahan J A, Doerfert J, Granzow J, Heckmann P H and Hutton R 1996 *J. Phys. B: At. Mol. Opt. Phys.* **29** 2647–59

[41] Hutton R, Engström L and Träbert E 1988 *Nucl. Instrum. Methods Phys. Res.* B **31** 294–9

[42] Savitzky A and Golay M J E 1964 *Anal. Chem.* **36** 1627–39

[43] Curtis L J 1991 *Phys. Scr.* **43** 137–43

[44] Curtis L 1992 *J. Opt. Soc. Am.* **9** 5–9

[45] Curtis L J, Matulioniene R, Ellis D G and Froese Fischer C 2000 *Phys. Rev.* A **62** 052513 1–7

[46] Curtis L J, Ellis D G and Martinson I 1995 *Phys. Rev.* A **51** 251–6

[47] Liljeby L, Lindgård A, Mannervik S, Veje E and Jelenkovic B 1979 *Phys. Scr.* **21** 805

[48] Kernahan J A, Pinnington E H, O'Neill J A, Brooks R L and Donnelly K E 1979 *Phys. Scr.* **19** 267–70

[49] Biémont E, Dumont P-D, Garnir H P, Palmeri P and Quinet P 2002 *Eur. J. Phys.* **20** 199–204

[50] Martinson I, Curtis L J, Huldt S, Litzén U, Liljeby L, Mannervik S and Jelenkovic B 1979 *Phys. Scr.* **19** 17–21

[51] Andersen T, Eriksen P, Poulsen O and Ramanujam P S 1979 *Phys. Rev.* A **20** 2621–4

[52] Kaufman V and Sugar J 1987 *J. Opt. Soc. Am.* **4** 1919–23

[53] Lurio A and Novick R 1964 *Phys. Rev.* **134** A608–14

[54] Ansbacher W, Pinnington E H, Kernahan J A and Gosselin R N 1986 *Can. J. Phys.* **64** 1365–8

[55] Pinnington E H, Kernahan J A and Ansbacher W 1987 *Can. J. Phys.* **65** 7–12

[56] Pinnington E H, Ansbacher W, Kernahan J A, Gosselin R N, Bahr J L and Inamdar A S 1985 *J. Opt. Soc. Am.* B **2** 1653–7

[57] Pinnington E H, Ansbacher W and Kernahan J A 1987 *J. Opt. Soc. Am.* B **4** 696–7

[58] Pinnington E H, Ansbacher W, Kernahan J A and Inamdar A S 1985 *J. Opt. Soc. Am.* B **2** 331–5

[59] Ansbacher W, Pinnington E H, Tauheed A and Kernahan J A 1991 *J. Phys. B: At. Mol. Opt. Phys.* **24** 587–93

[60] O'Neill J A, Pinnington E H, Donnelly K E and Brooks R L 1979 *Phys. Scr.* **20** 60–4

[61] Kernahan J A, Pinnington E H, O'Neill J A, Bahr J L and Donnelly K E 1980 *J. Opt. Soc. Am.* **70** 1126–30

[62] Moore C E 1952 *Atomic Energy Levels* vol 3 NSRDS-NBS 35 (Reissued: December 1971)

[63] Andersen T and Sørensen G 1973 *J. Quant. Spectrosc. Radiat. Transfer* **13** 369–76

[64] Lurio A 1965 *Phys. Rev.* A **140** A1505–8

[65] Skerbele A and Lassetre E N 1972 *J. Chem. Phys.* **52** 2708–11

[66] Abjean R and Johannin-Gilles A 1976 *J. Quant. Spectrosc. Radiat. Transfer* **16** 369–71

[67] Pinnington E H, Ansbacher W, Kernahan J A, Ahmad T and Ge Z-Q 1988 *Can. J. Phys.* **66** 960–2

[68] Jean P, Martin M and Lecler D 1967 *C. R. Seances Acad. Sci. Ser.* B **264** 1709–12

[69] Henderson M and Curtis L J 1996 *J. Phys. B: At. Mol. Opt. Phys.* **29** L629–34

[70] Ansbacher W, Pinnington E H and Kernahan J A 1988 *Can. J. Phys.* **66** 402–4

[71] Ansbacher W, Pinnington E H, Tauheed A and Kernahan J A 1989 *Phys. Scr.* **40** 454–6

[72] Frage S, Karwowski J and Saxena K M A 1976 *Handbook of Atomic Data* (Amsterdam: Elsivier)

[73] Cowan R D 1981 *The Theory of Atomic Structure and Spectra* (Berkeley, CA: University of California Press)

[74] Biémont E, Garnir H P, Palmeri P, Li Z S and Svanberg S 2000 *Mon. Not. R. Astron. Soc.* **312** 116–22

[75] Henderson M, Curtis L J, Matulioniene R, Ellis D G and Theodosiou C E 1997 *Phys. Rev.* A **56** 1872–8

[76] Norby L J 1991 *J. Chem. Educ.* **68** 110–3

[77] Pyykkö P 1988 *Chem. Rev.* **88** 563–94